Monthly Notices
of the
ROYAL ASTRONOMICAL SOCIETY

MNRAS **484,** 4718–4725 (2019)
Advance Access publication 2019 February 04

doi:10.1093/mnras/stz317

Spectroscopic detection of multiple populations in the ∼2 Gyr old cluster Hodge 6 in the LMC

K. Hollyhead,[1★] S. Martocchia,[2,3] C. Lardo,[4] N. Bastian,[3] N. Kacharov,[5] F. Niederhofer,[6] I. Cabrera-Ziri,[7†] E. Dalessandro,[8] A. Mucciarelli,[9] M. Salaris[3] and C. Usher[3]

[1]*Department of Astronomy, Oscar Klein Centre, Stockholm University, AlbaNova, Stockholm SE-106 91, Sweden*
[2]*European Southern Observatory, Karl-Schwarzschild-Straße 2, D-85748 Garching bei Mu¨nchen, Germany*
[3]*Astrophysics Research Institute, Liverpool John Moores University, 146 Brownlow Hill, Liverpool L3 5RF, UK*
[4]*Laboratoire d'astrophysique, Ecole Polytechnique Fèdèrale de Lausanne (EPFL), Observatoire de Sauverny, CH-1290 Versoix, Switzerland*
[5]*Max-Planck-Institut für Astronomie, Königstuhl 17, D-69117 Heidelberg, Germany*
[6]*Leibniz-Institut für Astrophysik Potsdam, An der Sternwarte 16, D-14482 Potsdam, Germany*
[7]*Harvard-Smithsonian Center for Astrophysics, 60 Garden Street, Cambridge, MA 02138, USA*
[8]*INAF, Osservatorio Astronomico di Bologna, via Ranzani 1, I-40127 Bologna, Italy*
[9]*Department of Physics and Astronomy, University of Bologna, Viale Berti Pichat 6/2, I-40127 Bologna, Italy*

Accepted 2019 January 28. Received 2019 January 12; in original form 2018 June 12

ABSTRACT

We report the spectroscopic discovery of abundance spreads (i.e. multiple populations) in the ∼2 Gyr old cluster in the LMC, Hodge 6. We use low-resolution VLT FORS2 spectra of 15 member stars in the cluster to measure their *CN* and *CH* band strengths at ≃3883 and 4300 Å, respectively, as well as [C/Fe] and [N/Fe] abundances. We find a subpopulation of two stars that are enriched in nitrogen, and we conclude that this subpopulation is evidence of multiple populations in Hodge 6. This is the second ∼2 Gyr old cluster (the first being NGC 1978 in the LMC) to show multiple populations and the first spectroscopic detection of MPs in a cluster of this age. This result is interesting as it hints at a possible relationship between the disappearance of extended main sequence turn-offs in clusters younger than ∼2 Gyr and the onset of multiple populations at ∼2 Gyr, which should be explored further.

Key words: Magellanic Clouds – galaxies: star clusters: individual: Hodge 6.

1 INTRODUCTION

Multiple populations (MPs), chemical variations (e.g. O-Na, C-N anticorrelations), and splits/spreads in colour–magnitude diagrams, which are ubiquitous to globular clusters (e.g. Carretta et al. 2009; Mucciarelli et al. 2009; Gratton, Carretta & Bragaglia 2012; Piotto et al. 2015) have recently been identified in intermediate-age (2–8 Gyr) massive clusters in the small and large magellanic clouds (SMC/LMC), spanning this full range of ages. These include Lindsay 1 (∼8 Gyr; Hollyhead et al. 2017; Niederhofer et al. 2017), Kron 3, NGC 416, and NGC 339 (∼6 Gyr old; Niederhofer et al. 2017; Hollyhead et al. 2018). Most recently, the ∼2 Gyr old cluster NGC 1978 was shown to have evidence of a split red giant branch (RGB) and subgiant branch in its colour–magnitude diagram (CMD; Martocchia et al. 2018a,b).

Clusters younger than ∼2 Gyr, though of comparable mass to the aforementioned SMC clusters and globular clusters (GCs), show a lack of evidence for MPs spectroscopically (e.g. NGC 1806; Mucciarelli et al. 2014) and photometrically (e.g. NGC 419; Martocchia et al. 2017). Interestingly, open clusters of comparable ages and masses to clusters with MPs have been found to lack MPs in some cases (e.g. Berkeley 39 and NGC 6791, masses $\sim 10^4$ $M_\odot$, ages 6 and 7–8 Gyr, respectively; Kassis et al. 1997; Platais et al. 2011; Bragaglia et al. 2012, 2014; Brogaard et al. 2012), and show evidence in others (Pancino 2018). Having sufficient mass is known to be a key factor in whether or not a cluster forms MPs (Carretta et al. 2010; Schiavon et al. 2013; Milone et al. 2017), with the lowest mass GCs that host MPs being $10^{3.5-3.9}$ $M_\odot$ (Bragaglia et al. 2017; Milone et al. 2017; Simpson et al. 2017). However, the recent discoveries of MPs in intermediate-age clusters (∼2–8 Gyr), though not in young massive clusters (YMCs, <2 Gyr old) indicate that age also plays a key role. The precise mechanism of the formation of MPs and its direct relationship to age is still not fully understood (e.g. Bastian & Lardo 2018).

★ E-mail: kathie.hollyhead@astro.su.se
† Hubble fellow.

Despite a lack of evidence of MPs in YMCs spectroscopically, extended main-sequence turn-offs (eMSTOs) have been observed in many of their CMDs (e.g. Mackey & Broby Nielsen 2007; Piatti et al. 2014). This phenomenon is not observed in any clusters of any mass older than ∼2 Gyr. Though these observations were originally explained with an age spread in the cluster of 200–700 Myr (e.g. Milone et al. 2009), it has since been shown that this is unlikely due to the width of the turn-off being proportional to the age of the cluster (Niederhofer et al. 2015), and the discovery of extended turn-offs in clusters younger than the possible age spreads (e.g. NGC 1850, 100 Myr old; Bastian et al. 2016). Though it has been suggested that the spreads are related to the MP phenomenon as observed in GCs (e.g Goudfrooij et al. 2014), the size of the spreads and lack of eMSTO after ∼2 Gyr is described well by invoking stellar rotation (e.g. Bastian & de Mink 2009; Brandt & Huang 2015; D'Antona et al. 2015).

These discoveries have consequences for GC formation theories, which try to explain how MPs have formed. All current theories (e.g. Decressin et al. 2007; D'Ercole et al. 2008; Bastian et al. 2013) cannot fully explain observations (Bastian & Lardo 2015; Renzini et al. 2015) and have significant issues (e.g. mass–budget problem; Larsen, Strader & Brodie 2012; Kruijssen 2015). The detection of MPs in clusters down to ∼2 Gyr, however, helps to constrain these theories as it suggests the process should still be operating in the present-day Universe. This also means that YMCs can be used to constrain these theories, as they likely formed through the same mechanism. Studies of YMCs suggest that MPs should be formed in a single burst of star formation, due to a lack of gas reservoir to form a second generation (e.g. Cabrera-Ziri et al. 2015).

The aim of this project is to further investigate clusters around the age of ∼2 Gyr, which marks the point where clusters no longer have eMSTOs and where MPs have been identified in NGC 1978 (Martocchia et al. 2018b). By increasing the sample of clusters at this age, the onset of MPs can be further constrained and the relationship between the loss of eMTSOs and the appearance of MPs can be explored.

In this paper we analyse Hodge 6, a ∼2 Gyr cluster (Goudfrooij et al. 2014) in the LMC. Goudfrooij et al. (2014) give the mass of Hodge 6 as $8 \times 10^4\,M_\odot$ using a Salpeter IMF. If a Kroupa/Chabrier IMF is used Hodge 6 is $\sim 5 \times 10^4\,M_\odot$. This cluster was chosen for this study as it is shown to lack an eMSTO by Goudfrooij et al. (2014) and at ∼2 Gyr is at the limit where this phenomenon is observed, so can be used to explore the role this transition plays in the formation of MPs.

We have obtained low-resolution spectroscopy of lower RGB stars in the cluster in order to look for the signature of MPs in *CN* and *CH* band strengths (enrichment in N, e.g. Norris et al. 1981; Cohen, Briley & Stetson 2002; Kayser et al. 2008; Pancino et al. 2010; Lardo et al. 2012) that trace N and C, respectively. We also observed NGC 1978 on the same observing run; however after reduction and analysis, the data was deemed to be unusable, therefore we present only Hodge 6 in this paper. We discuss why NGC 1978 is not used and how we ensured that Hodge 6 data were still viable in Section 3.1.

In Section 2 we describe our data and briefly discuss the data reduction, while Section 3 describes how we differentiate between cluster members and field interlopers. The calculation of the *CN* and *CH* band strengths is discussed in Section 4, [C/Fe] and [N/Fe] calculations in Section 4.2, along with a new age estimate in Section 5. Finally, the results and discussion are included in Section 6.

2 OBSERVATIONS AND DATA REDUCTION

The data for Hodge 6 were obtained from FORS2 on the VLT at La Silla Paranal Observatory under the Programme ID 099.D-0762(B), P.I. K. Hollyhead. We used the same configuration as for previous observations for Lindsay 1 and Kron 3 (multi-object spectroscopy using the blue CCD in visitor mode with the 600B + 22 grism, in order to sample the *CN* and *CH* bands at 3839 and 4300 Å, respectively; Hollyhead et al. 2017, 2018). Three science exposures were obtained over the course of one half-night, covering 37 target stars across the two chips.

Pre-imaging was taken prior to the spectra under the same programme, obtaining *V* and *I* band images, which were used to select appropriate targets for the spectroscopy, in addition to calculating properties of the stars. The images were reduced using the REFLEX pipeline (Freudling et al. 2013), and point spread function (PSF) photometry was used to obtain magnitudes for stars within the images with DAOPHOT (Stetson 1987).

Targets for spectroscopic follow-up were selected from the CMD resulting from the PSF photometry. The targets were chosen from the stars along the RGB, with priority targets as those on the lower RGB and secondary targets closer to the tip. When the masks were produced for Hodge 6, secondary targets were selected only in the absence of primary targets, and where neither of these were available, random stars were selected to fill gaps.

The spectra were reduced using IRAF. The spectra were bias-subtracted, flat-fielded with a normalized flat-field image, cleaned of cosmic rays with the L.A COSMIC (van Dokkum 2001) routine and extracted. The 1D spectra were then wavelength calibrated and combined. The average *S*/*N* for our spectra is lower than for our previous studies, with averages of ∼11 and 16 for the *CN* and *CH* bands, respectively. Examples of the spectra are shown in Fig. 1.

3 CLUSTER MEMBERSHIP

We applied a number of different criteria to determine cluster membership. The process was the same as applied to the targets in Lindsay 1 and Kron 3 previously in Hollyhead et al. (2017, 2018).

First, a cut was made based on the radial velocities (RVs) of the targets. RVs were derived using IRAF. The star with the highest *S*/*N* was selected as the template spectrum for calculating the RVs of the other stars. The RVIDLINES routine was used to determine the RV of the template spectrum (star 11 on chip 1) as $264.8\,km\,s^{-1}$. The error on the RV measurements was estimated by measuring the RV of the template spectrum in RVIDLINES using lines at the bluer end of the spectrum compared to lines at the redder end as $\sim 30\,km\,s^{-1}$. Any stars more or less than $30\,km\,s^{-1}$ from the template RV were removed as non-members. This is shown in the top panel in Fig. 3 with each star's RV plotted against its distance from the centre of the cluster, and where the teal line is the template RV, and the blue shaded region indicates the acceptable range of velocities for member stars. The red points are likely non-members and the blue points are members.

In order to check that our template star was a member star itself, we looked at the histogram of the RVs, and star 11 was very close to the peak, and therefore likely a member. The histogram is shown in Fig. 2. The teal line shows the RV of star 11 and the blue shaded area is the selection of RVs, as described above. Our selection well samples the peak velocities while also missing a secondary peak of likely non-member stars at $\sim 200\,km\,s^{-1}$.

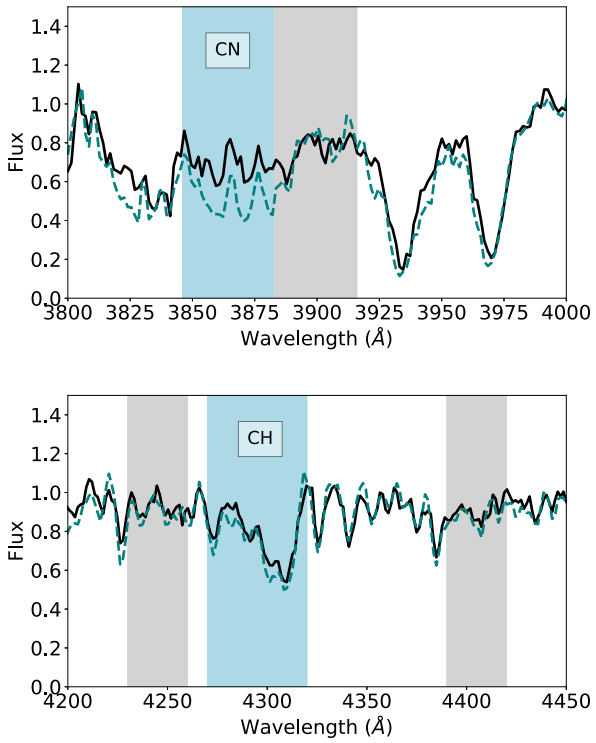

Figure 1. Examples of spectra in our sample. The spectra of a CN strong and a CN normal are shown in black and teal, respectively. They have both been continuum-normalized using IRAF. In the top plot we show the wavelength range including the *CN* band (shown in blue) and its continuum band (shown in grey). The lower plot shows the *CH* band. The two stars selected have similar properties (T_{eff} and magnitude) though they show a clear difference in their *CN* band.

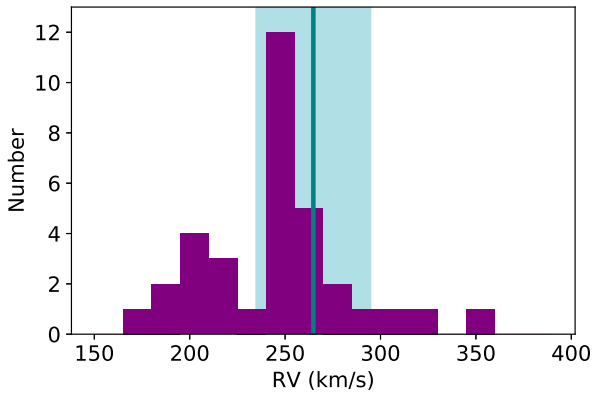

Figure 2. Histogram of the radial velocities of all stars with spectra in Hodge 6. The teal line shows the radial velocity found for our selected template star, indicating that it is very likely to be a member as it is close to the peak of RVs. The filled blue section shows the range over which we selected member stars.

The second panel in Fig. 3 shows estimates of the metallicity of each star, for which the strength of the Ca II (H + K) lines is a proxy. Once again, the blue points are members and the red points are non-members. Member stars were selected as those less than 2σ from the median of all stars, the same cut as applied for Kron 3 (Hollyhead et al. 2018). Previously we have used the Fe5270 band strengths, which are also proxies for metallicity, as a further criterion for membership. However, in this case no outliers

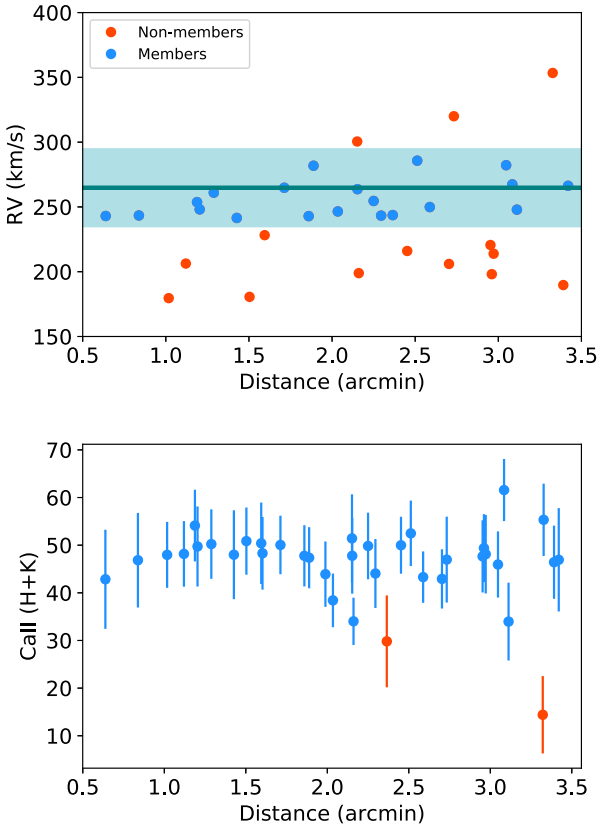

Figure 3. Here we show the criteria used to determine cluster membership for each of our stars. In all cases the blue stars were determined to be members from each test and the red points are non-members. They were cross-correlated and any star failing any of the three criteria was removed. The top panel shows the radial velocities of the stars against their distance from the centre of the cluster, with the RV of the template star as the teal line and the 30 km s^{-1} range by the shaded blue. Stars outside of this range were considered non-members. The second panel shows the Ca II (H + K) estimates for each star from band strengths. Stars outside of 2σ from the median were classified as non-members.

could be determined due to large errors, so it is not used for Hodge 6.

The CMD of the targets was then inspected to ensure no random filler stars were still considered members of the cluster. Fig. 4 shows the CMD using the photometry obtained from pre-imaging of the cluster. Grey points are all the sources within the catalogue, red points are the non-members, and blue points are members. Stars brighter than the bump were excluded from the final sample as the C and N abundances are significantly changed by internal mixing processes. Additionally several stars were too far to the right of the RGB and were removed. After applying all of these criteria, we were left with 15 member stars out of the total 37. All RVs and HK band strengths are listed in Table 1.

3.1 Bright star contamination

As mentioned previously, spectroscopy was also obtained for NGC 1978. This data could have been used as a further check of our method for determining MPs, as they have been shown to be present in *HST* photometry. However, during the reduction of the data we discovered that most of the member stars' spectra were contaminated by nearby bright stars, therefore making the data unreliable and unusable for this study.

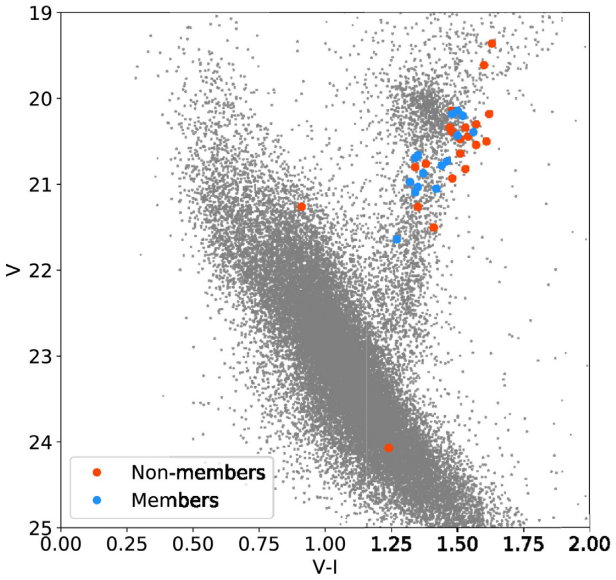

Figure 4. CMD of all the stars in the pre-imaging field for Hodge 6, with photometry obtained using DAOPHOT (Stetson 1987). The grey points are all stars in the photometry, while member stars with spectroscopy are shown as blue points and non-members (determined from the CMD and other sources) are shown as red points.

After this was found, we checked the spectra for Hodge 6 to ensure that the data for this cluster was viable. By examining the spectra, images, and the brightness and colour of all sources within 5 arcsec, we determined that 10 of our 15 member stars were uncontaminated or had only very faint stars nearby. We also checked *HST* ACS images of the cluster for a more thorough check of any stars within the field of view.

4 BAND STRENGTHS AND ABUNDANCES

4.1 *CN* and *CH* band strengths

We have calculated the band strengths Sλ3883 (CN) and CHλ4300 (CH) to investigate the presence of multiple populations in Hodge 6. This technique has been used previously for Milky Way Globular Clusters (e.g. Pancino et al. 2010) and for our other intermediate-age clusters Lindsay 1 and Kron 3 (Hollyhead et al. 2017, 2018).

The band strengths are calculated using the definitions in Norris et al. (1981), Worthey (1994), and Lardo et al. (2013). Errors on each measurement are calculated as per Vollmann & Eversberg (2006). The bands used for the calculations, including the ranges used as estimates of the continuum for each band are shown in Fig. 1, with blue as the molecular band and grey as the continuum bands. Our values for the *CN* and *CH* band strengths for each star are listed in Table 1.

4.2 [C/Fe] and [N/Fe]

We also derived [C/Fe] and [N/Fe] abundances for the 10 uncontaminated member stars using the same methods as for previous clusters Lindsay 1 and Kron 3. We carried out spectral synthesis using the same bands as for the band strength determinations to obtain estimates of [C/Fe] and [N/Fe].

We used Kurucz line lists taken from the website of F. Castelli[1] and used ATLAS9 to produce model atmospheres using [Fe/H] $= -0.3$ (Goudfrooij et al. 2014) and the parameters derived for each star. Effective temperture was found using a $T_{\rm eff}$–colour calibration (Alonso, Arribas & Martínez-Roger 1999) with V–I, using our pre-imaging photometry. Surface gravities were calculated using a distance modulus of 18.4 (Goudfrooij et al. 2014), the previously determined effective temperatures, and bolometric corrections also from Alonso et al. (1999).

Kurucz's SYNTHE code was used to create model spectra, which were used in a χ^2 minimization with the observed spectra to find the abundances. Measured [C/Fe] abundances were used in finding [N/Fe] across the *CN* band, with solar abundances taken from Asplund et al. (2009). In order to calculate uncertainties from the fitted parameters, we iteratively change one parameter and repeat the abundance analyses for the full range of temperatures and gravities, as used in Lardo et al. (2013). Error introduced from the χ^2 fitting procedure (found by re-fitting after introducing Poissonian noise) is added in quadrature to give the final errors in Table 1. We find very large errors due to the noise in the spectra at the bands used, and the difficulty in calculating [C/Fe] and [N/Fe] using molecular bands, rather than individual lines.

5 THE AGE OF HODGE 6

In order to more accurately determine the age of Hodge 6, which is not greatly discussed in the literature, we fit a CMD produced with existing photometry of Hodge 6 (Goudfrooij et al. 2014), which was field star subtracted as per Niederhofer et al. (2017). Fig. 5 shows the CMD in the F475W and F814W filters with the best-fitting BaSTI isochrone (parameters age = 2 Gyr, [Fe/H] = −0.35 dex, distance modulus = 18.5 and Av = 0.22; Pietrinferni et al. 2006), giving Hodge 6 an age of ∼2 Gyr.

We have also directly compared the CMD of Hodge 6 with that of NGC 1978, though the blue filter differs between the two observations (i.e. F475W versus F555W). Comparing the two (with F814W on the y-axis, which is common between the two) led us to conclude that the two clusters were coeval within ∼200 Myr. As discussed previously, Martocchia et al. (2018a,b) found MPs within NGC 1978 and estimated an age of ∼2 Gyr based on isochrone fitting.

6 RESULTS AND DISCUSSION

In Fig. 6 we show the distribution of *CN* and *CH* band strengths for all non-contaminated member stars, as listed in Table 1. The stars show a similar result to that observed for Kron 3 and Lindsay 1; a spread in CN, which traces nitrogen (∼0.7 mag), with negligible spread in *CH*, which traces carbon. We interpret this result to be evidence for multiple populations in Hodge 6. The blue points are the non-enriched stars and the three purple points indicate the N-enriched subpopulation, which we identify as more than 1σ from the median of the CN distribution.

To further test the distribution of stars in CN/CH space and confirm that the three enriched stars are a separate population, we also ran a KMeans clustering algorithm on the data set using the SKLEARN package in PYTHON. In the left-hand plot of Fig. 7 we show the results of running the algorithm with 1-4 numbers of clusters. When a two cluster solution is requested, the algorithm selects

[1] http://wwwuser.oats.inaf.it/castelli/linelists.html

Table 1. Properties of all the stars in our data set. ID refers to the ID for the star within our complete photometric catalogue. RVs are those calculated as in Section 3, HK refers to the Ca II (H + K) metallicity proxy, CN and CH are our band strengths, [C/Fe] and [N/Fe] are abundances, and 'Member' refers to which stars we found to be cluster members and non-members. A 1 indicates that the star is a member, 0 indicates that it is a non-member. 'Cont' refers to whether the star was found to be contaminated by bright sources or not, a 1 is contaminated and a 0 is not contaminated. Finally, 'Enriched' indicates whether the star has N enrichment or not. 1 means the star is enriched, 0 means it is non-enriched.

ID	RA	Dec	V (mag)	I (mag)	RV (km s^{-1})	HK (mag)	CN	CH	[C/Fe]	[N/Fe]	Member	Cont	Enriched
15219	85.5362524	−71.5351338	21.09 ± 0.02	19.75 ± 0.01	266	46.9 ± 10.8	−0.03 ± 0.07	−0.32 ± 0.12	−0.34 ± 0.22	−0.48 ul	1	0	0
9794	85.6095721	−71.5429143	20.69 ± 0.02	19.35 ± 0.01	214	48.1 ± 8.2	0.15 ± 0.08	−0.39 ± 0.08	–	–	0	N/A	N/A
8311	85.6300597	−71.5533655	20.14 ± 0.01	18.66 ± 0.01	286	52.5 ± 6.9	0.42 ± 0.08	−0.35 ± 0.1	−0.45 ± 0.20	0.34 ± 0.27	1	0	1
11665	85.5840111	−71.5553459	20.34 ± 0.01	18.87 ± 0.01	301	51.4 ± 9.3	0.13 ± 0.06	−0.36 ± 0.08	–	–	0	N/A	N/A
9522	85.6134158	−71.5575938	20.43 ± 0.01	18.93 ± 0.01	264	47.8 ± 7.9	−0.05 ± 0.05	−0.39 ± 0.08	−0.33 ± 0.20	−0.70 ul	1	0	0
14926	85.5403979	−71.5642641	20.20 ± 0.01	18.68 ± 0.01	265	50.0 ± 6.1	0.13 ± 0.08	−0.36 ± 0.08	−0.39 ± 0.20	0.00 ± 0.27	1	0	0
8490	85.6274101	−71.5710060	20.14 ± 0.01	18.64 ± 0.01	228	50.4 ± 8.5	0.17 ± 0.09	−0.32 ± 0.12	–	–	0	N/A	N/A
17152	85.5095419	−71.5664829	20.39 ± 0.01	18.91 ± 0.01	282	47.4 ± 6.4	0.08 ± 0.06	−0.38 ± 0.09	−0.44 ± 0.20	−0.32 ± 0.27	1	0	0
20569	85.4611624	−71.5775750	20.18 ± 0.01	18.70 ± 0.01	255	49.8 ± 7.0	0.25 ± 0.07	−0.36 ± 0.08	−0.24 ± 0.19	0.12 ± 0.27	1	0	1
9065	85.6197799	−71.5757263	21.05 ± 0.01	19.63 ± 0.01	261	50.2 ± 7.3	0.33 ± 0.13	−0.38 ± 0.11	–	–	1	1	1
8131	85.6328257	−71.5852180	20.78 ± 0.01	19.34 ± 0.01	248	49.7 ± 8.4	0.18 ± 0.08	−0.39 ± 0.11	–	–	1	1	0
8027	85.6343877	−71.5890848	20.30 ± 0.01	18.73 ± 0.01	254	54.1 ± 7.5	0.47 ± 0.11	−0.37 ± 0.1	–	–	0	N/A	N/A
7152	85.6470162	−71.5930918	20.73 ± 0.01	19.27 ± 0.01	242	48.0 ± 9.3	0.08 ± 0.11	−0.39 ± 0.09	−0.48 ± 0.20	−0.07 ± 0.27	1	0	0
9461	85.6142583	−71.5951287	21.03 ± 0.01	19.68 ± 0.01	243	46.8 ± 9.9	0.1 ± 0.1	−0.38 ± 0.11	–	–	1	1	0
13362	85.5616156	−71.5808774	20.97 ± 0.01	19.65 ± 0.01	243	42.8 ± 10.4	0.01 ± 0.08	−0.46 ± 0.1	−0.58 ± 0.22	−0.18 ± 0.30	1	0	0
12838	85.5688218	−71.5478795	20.66 ± 0.01	19.31 ± 0.01	250	43.3 ± 5.4	0.07 ± 0.08	−0.39 ± 0.09	−0.58 ± 0.22	−0.25 ± 0.30	1	0	0
19789	85.4722555	−71.5511889	20.39 ± 0.01	18.91 ± 0.01	282	45.9 ± 6.9	0.02 ± 0.06	−0.38 ± 0.07	−0.27 ± 0.19	−0.09 ± 0.27	1	0	0
12852	85.5686579	−71.5454685	21.26 ± 0.01	19.91 ± 0.01	320	47.0 ± 9.0	0.1 ± 0.08	−0.39 ± 0.1	–	–	0	N/A	N/A
6987	85.6495882	−71.5675732	21.26 ± 0.01	20.35 ± 0.01	247	38.4 ± 5.6	−0.1 ± 0.03	−0.49 ± 0.06	–	–	0	N/A	N/A
10063	85.6056276	−71.5407052	19.36 ± 0.01	17.73 ± 0.01	267	61.6 ± 6.5	0.55 ± 0.09	−0.34 ± 0.12	–	–	0	N/A	N/A
6192	85.6125426	−71.6045965	20.34 ± 0.02	18.81 ± 0.01	206	48.2 ± 6.9	0.19 ± 0.07	−0.39 ± 0.09	–	–	0	N/A	N/A
7847	85.5763716	−71.6078986	20.82 ± 0.02	19.29 ± 0.01	180	48.0 ± 6.9	0.26 ± 0.1	−0.36 ± 0.11	–	–	0	N/A	N/A
4211	85.6575364	−71.6102169	20.64 ± 0.02	19.13 ± 0.01	−12	43.9 ± 6.9	−0.01 ± 0.04	−0.42 ± 0.07	–	–	0	N/A	N/A
8384	85.5650453	−71.6159635	20.50 ± 0.02	18.89 ± 0.01	181	50.9 ± 7.1	0.32 ± 0.1	−0.36 ± 0.1	–	–	0	N/A	N/A
9409	85.5426523	−71.6205717	20.54 ± 0.02	18.97 ± 0.01	243	47.8 ± 6.4	0.14 ± 0.09	−0.35 ± 0.1	–	–	0	N/A	N/A
3662	85.6704510	−71.6236386	20.44 ± 0.02	18.90 ± 0.01	206	42.9 ± 6.2	0.16 ± 0.06	−0.37 ± 0.1	–	–	0	N/A	N/A
10665	85.5147734	−71.6260383	21.50 ± 0.02	20.09 ± 0.01	244	29.8 ± 9.6	−0.17 ± 0.05	−0.49 ± 0.08	–	–	0	N/A	N/A
4558	85.6497866	−71.6338156	20.47 ± 0.02	18.96 ± 0.01	198	49.4 ± 7.1	0.23 ± 0.05	−0.37 ± 0.09	–	–	0	N/A	N/A
7553	85.5829425	−71.6290964	20.87 ± 0.02	19.50 ± 0.01	243	44.1 ± 7.2	0.07 ± 0.06	−0.44 ± 0.09	–	–	1	1	0
9237	85.5462846	−71.6395408	20.39 ± 0.02	18.83 ± 0.01	221	47.7 ± 7.6	0.15 ± 0.07	−0.38 ± 0.1	–	–	0	N/A	N/A
10758	85.5129849	−71.6443645	20.76 ± 0.02	19.38 ± 0.01	190	46.4 ± 7.7	0.36 ± 0.08	−0.36 ± 0.1	–	–	0	N/A	N/A
7246	85.5892943	−71.6315025	20.18 ± 0.03	18.56 ± 0.01	216	50.0 ± 6.0	0.29 ± 0.1	−0.37 ± 0.11	–	–	0	N/A	N/A
10150	85.5264974	−71.6135182	20.93 ± 0.02	19.45 ± 0.01	136	48.3 ± 7.6	0.11 ± 0.08	−0.38 ± 0.1	–	–	0	N/A	N/A
4671	85.6471151	−71.6181124	19.61 ± 0.02	18.01 ± 0.01	199	34.0 ± 5.0	−0.11 ± 0.03	−0.43 ± 0.05	–	–	0	N/A	N/A
3581	85.6724476	−71.6365114	20.80 ± 0.02	19.46 ± 0.01	353	55.3 ± 7.6	0.36 ± 0.08	−0.35 ± 0.11	–	–	0	N/A	N/A
9607	85.5384326	−71.6417748	21.64 ± 0.03	20.37 ± 0.01	248	34.0 ± 8.2	−0.16 ± 0.06	−0.48 ± 0.07	–	–	1	1	0
8419	85.5580955	−71.6461893	24.07 ± 0.05	22.83 ± 0.02	2709	14.4 ± 8.1	−0.32 ± 0.03	−0.55 ± 0.06	–	–	0	N/A	N/A

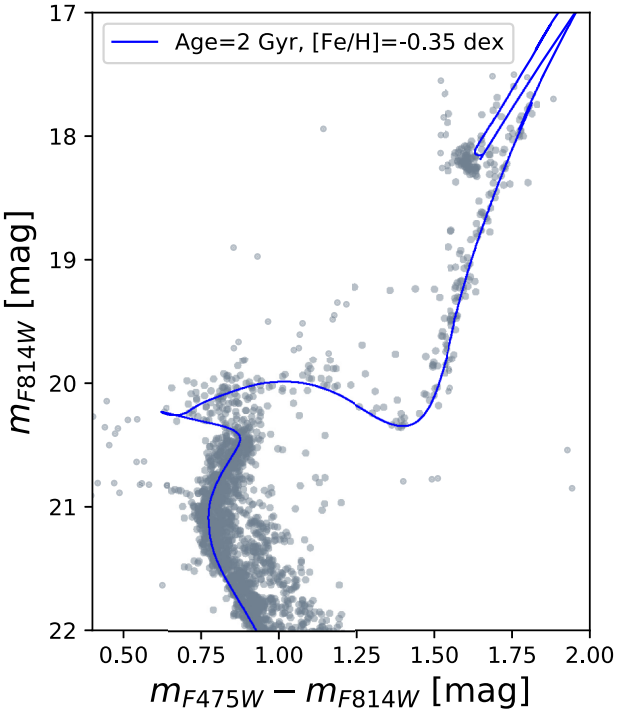

Figure 5. CMD for Hodge 6 constructed with ACS photometry in F475W and F814W filters. The CMD has been field star subtracted. The best-fitting BaSTI isochrone is shown, giving Hodge 6 an age of ∼2 Gyr and [Fe/H] of −0.35 dex.

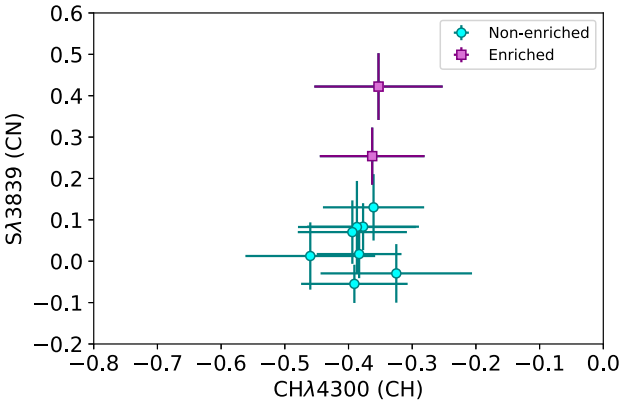

Figure 6. CN versus CH for all member stars in Hodge 6. A spread of ∼0.7 mag in N is much larger than the negligible spread in C. The purple points indicate the enriched stars, more than 1σ from the median of the population. The blue points are non-enriched stars.

the same three CN-enhanced stars as a separate group to the rest, in agreement with our initial selection. However, as the number of clusters is selected, this does not mean that 2 is the optimal number of clusters for the data. To check this, we use the elbow test, where we plot the inertia (the average distance of each point to their cluster centre) against the number of clusters, as shown in the right-hand plot in Fig. 7. The largest change in gradient between points indicates the best option for the number of clusters, in this case 2.

The spectra in Fig. 1 also clearly show the differences between spectra of CN-enhanced and non-enriched stars. We selected one CN-enriched star and one non-enriched star with very similar properties (i.e. magnitude) for the plot to show the difference in their *CN* band. The figure clearly shows that the enriched star in teal has enhanced CN, whereas both stars have very similar absorption in the *CH* band, in agreement with Fig. 6 that shows a spread in CN with no corresponding spread in CH.

This difference between CH and CN is also shown in Fig. 8. Here we show CH and CN, respectively, against *V*- band magnitude. Again, the axes cover the same range in order to illustrate the difference. We fit the points with a straight line (shown in black) and show the distributions of the residuals of the fit in the inner plots. The histograms are fitted with the MIXED GAUSSIAN routine in the SKLEARN package in PYTHON.

Fig. 9 shows our estimates of the [C/Fe] and [N/Fe] abundances for all non-contaminated member stars. Though the errors are very large and make it difficult to interpret any definite results, we can still roughly see a larger spread in [N/Fe] than [C/Fe], as mirrored in the CN/CH distribution. Additionally, the two purple points indicate the CN-enriched stars selected from the CN/CH plot, which also have higher [N/Fe] than the other points. Therefore this indicates that CN does reliably trace nitrogen abundance.

The method using *CN* and *CH* band strengths to investigate MPs is reliable, as it shows the expected results for Milky Way GCs (Kayser et al. 2008; Pancino et al. 2010) and our previous result with Lindsay 1 (Hollyhead et al. 2017) using the same process was also confirmed with *HST* photometry (Niederhofer et al. 2017). The technique has an advantage over high-resolution spectroscopy, which would be required for accurate [C/Fe] and [N/Fe] (though they can be estimated), in allowing for a larger sample of stars to be observed in less time. Looking for MPs requires a fairly large number of stars in order to ensure any enriched stars are not missed, as in some clusters the enriched population appears to be more centrally concentrated (Lardo et al. 2011; Dalessandro et al. 2016; Simioni et al. 2016). Unlike photometry, however, this method is limited by the central regions of the cluster that are too crowded to sample, meaning the ratio of enriched to non-enriched stars cannot reliably be estimated from spectroscopy.

Fig. 10 shows the relationship between cluster age, mass, and the presence of MPs. This plot illustrates that MPs are present in all clusters of sufficient mass down to the age of ∼2 Gyr. Below this age, clusters show no spectroscopic or photometric evidence for MPs. The confirmation of the presence of MPs in clusters at ∼2 Gyr old such as Hodge 6 or NGC 1978 (Martocchia et al. 2018a,b) has significant consequences for GC formation theories, as it means the mechanism must still be operating in the present day.

This apparent age limit for MPs is also interesting due to its coincidence with the disappearance of eMSTOs, which are observed in clusters younger than ∼2 Gyr, but none older. Hodge 6 does not show a prominent eMSTO, as the width of the turn-off has been estimated as $\sigma < 100$ Myr (Goudfrooij et al. 2014).

The apparent coincidence of the lack of eMSTOs and the beginning of MPs could well be just that – a coincidence. Relatively very few numbers of clusters have been studied at this exact age limit and so there is not the statistical consensus to indicate that these two phenomena are related, though studies so far do point to an age dependence on the onset of MPs.

Further study of clusters at this age limit is needed to determine whether these two phenomena are related. If eMSTOs can predict which young clusters will develop MPs, these objects can be used to determine the mechanism for the onset of MPs. Our result also suggests that YMCs can be considered analogues to GCs and used to determine their formation.

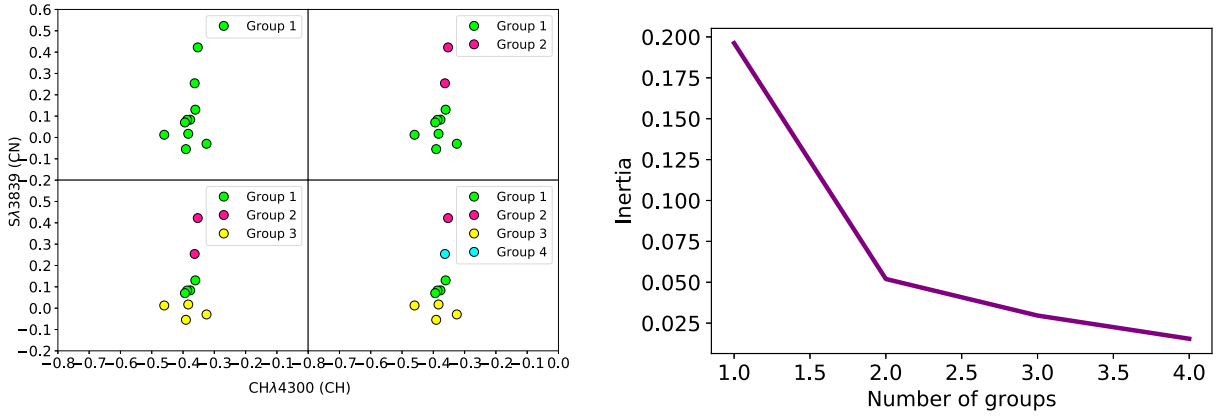

Figure 7. Results of the KMeans clustering algorithm ran on our data. The left-hand plot shows the identified groups for inputs of 1-4 clusters, while the right-hand plot shows the average distance between each group member and their cluster centre (inertia), used to find the optimal number of clusters.

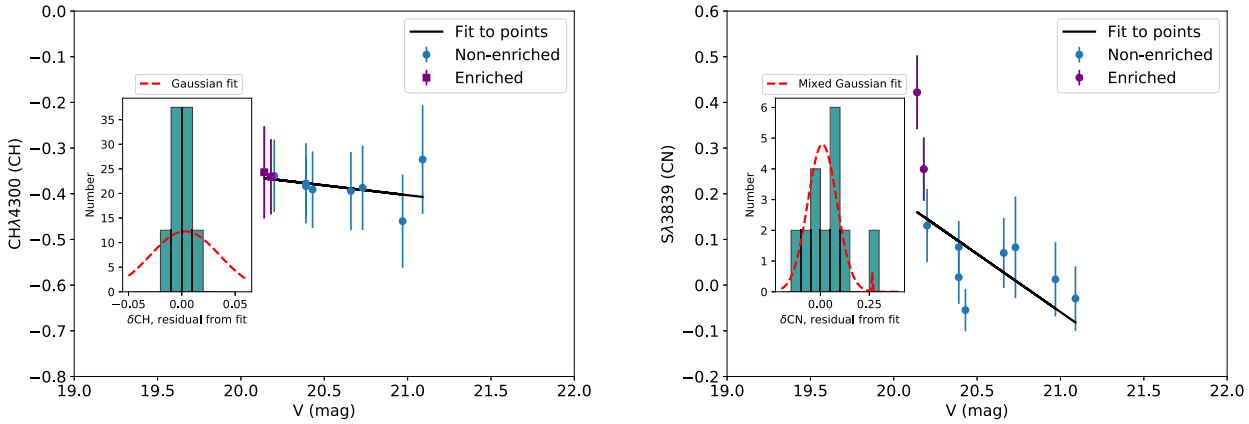

Figure 8. CH and CN plotted against *V* band magnitude for all member stars. N-enriched stars identified from the CN/CH plot are shown in purple. The data is fit in each case with a straight line (black line) and the inner plots show the residuals of each point from the fit.

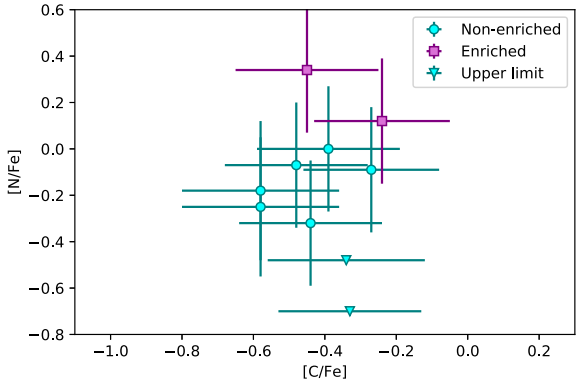

Figure 9. [C/Fe] and [N/Fe] for all member non-contaminated stars. As with CN and CH we see a spread in [N/Fe] without a spread in [C/Fe]. This shows that our stars enriched in CN are also enriched in [N/Fe] and therefore CN is representative of nitrogen abundance. The errors are very large on these estimations due to low-resolution spectra and high amounts of noise. The purple squares are enriched stars (selected from CN/CH), the blue circles are non-enriched stars, and the blue triangles are non-enriched stars but with only upper limits on the measurements of [N/Fe].

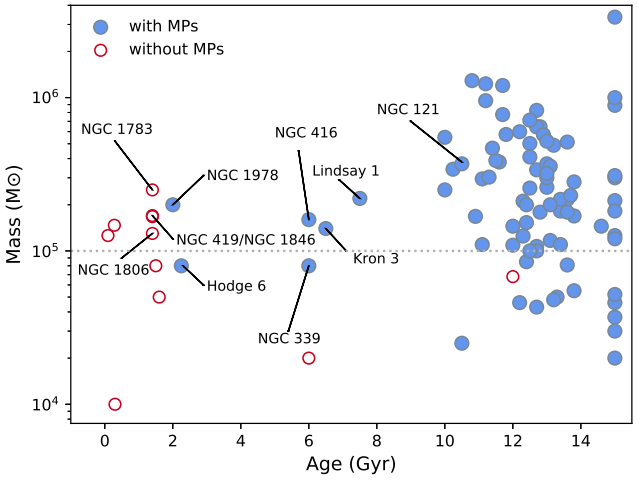

Figure 10. Age versus mass for all clusters studied so far looking for the presence of multiple populations. The filled circles indicate clusters where MPs are found and empty circles are those without MPs. The plot indicates that age plays a clear role in whether a cluster has MPs or not, with the transition from MPs to none occurring at the age at which the eMSTO phenomenon is no longer observed.

This coincidence could potentially be related to the mass of the stars on the RGB when abundances of these stars are measured. The ∼2 Gyr age limit also corresponds to the mass of RGB stars changing to lower mass stars of $\sim 1.5\,M_{\odot}$. Therefore, the observation of MPs in clusters is related to the mass of the stars that are observed and less evolved stars would need to be studied in clusters younger than ∼2 Gyr. There is evidence, however, that there is an increase in the observability of MPs with age (Martocchia et al. 2018b), and ∼2 Gyr may be the youngest age where they are observable.

Finally, as said previously, the sample of clusters that are studied for this purpose is fairly small and constrained to the local Universe. Improving our ability to study clusters to greater distances and therefore sampling a wider range of environments would be highly beneficial to interpreting these results and discovering the mechanism for the onset of MPs.

ACKNOWLEDGEMENTS

Based on observations made with ESO telescopes at the La Silla Paranal Observatory under Programme ID 099.D-0762(B), P.I. K Hollyhead.

We thank P. Goudfrooij for making the *HST* photometry of Hodge 6 available to us.

C. Lardo thanks the Swiss National Science Foundation for supporting this research through the Ambizione grant number PZ00P2 168065.

N. Bastian gratefully acknowledges financial support from the Royal Society (University Research Fellowship) and the European Research Council (ERC-CoG-646928-Multi-Pop).

F. Niedernofer acknowledges support from the European Research Council (ERC) under European Union's Horizon 2020 research and innovation programme (grant agreement No 682115).

Support for this work was provided by NASA through Hubble Fellowship grant *HST*-HF2-51387.001-A awarded by the Space Telescope Science Institute, which is operated by the Association of Universities for Research in Astronomy, Inc., for NASA, under contract NAS5-26555.

C. Usher gratefully acknowledges financial support from European Research Council (ERC-CoG-646928-Multi-Pop).

REFERENCES

Alonso A., Arribas S., Martínez-Roger C., 1999, A&AS, 140, 261
Asplund M., Grevesse N., Sauval A. J., Scott P., 2009, ARA&A, 47, 481
Bastian N., de Mink S. E., 2009, MNRAS, 398, L11
Bastian N., Lardo C., 2015, MNRAS, 453, 357
Bastian N., Lardo C., 2018, Annu. Rev. Astron. Astrophys., 56, 83
Bastian N., Lamers H. J. G. L. M., de Mink S. E., Longmore S. N., Goodwin S. P., Gieles M., 2013, MNRAS, 436, 2398
Bastian N. et al., 2016, MNRAS, 460, L20
Bragaglia A., Gratton R. G., Carretta E., D'Orazi V., Sneden C., Lucatello S., 2012, A&A, 548, A122
Bragaglia A., Sneden C., Carretta E., Gratton R. G., Lucatello S., Bernath P. F., Brooke J. S. A., Ram R. S., 2014, ApJ, 796, 68
Bragaglia A., Carretta E., D'Orazi V., Sollima A., Donati P., Gratton R. G., Lucatello S., 2017, A&A, 607, A44
Brandt T. D., Huang C. X., 2015, ApJ, 807, 25
Brogaard K. et al., 2012, A&A, 543, A106
Cabrera-Ziri I. et al., 2015, MNRAS, 448, 2224
Carretta E. et al., 2009, A&A, 505, 117
Carretta E., Bragaglia A., Gratton R. G., Recio- Blanco A., Lucatello S., D'Orazi V., Cassisi S., 2010, A&A, 516, A55
Cohen J. G., Briley M. M., Stetson P. B., 2002, AJ, 123, 2525
D'Antona F., Di Criscienzo M., Decressin T., Milone A. P., Vesperini E., Ventura P., 2015, MNRAS, 453, 2637
D'Ercole A., Vesperini E., D'Antona F., McMillan S. L. W., Recchi S., 2008, MNRAS, 391, 825
Dalessandro E., Lapenna E., Mucciarelli A., Origlia L., Ferraro F. R., Lanzoni B., 2016, ApJ, 829, 77
Decressin T., Meynet G., Charbonnel C., Prantzos N., Ekström S., 2007, A&A, 464, 1029
Freudling W., Romaniello M., Bramich D. M., Ballester P., Forchi V., García-Dabló C. E., Moehler S., Neeser M. J., 2013, A&A, 559, A96
Goudfrooij P. et al., 2014, ApJ, 797, 35
Gratton R. G., Carretta E., Bragaglia A., 2012, A&AR, 20, 50
Hollyhead K. et al., 2017, MNRAS, 465, L39
Hollyhead K. et al., 2018, MNRAS, 476, 114
Kassis M., Janes K. A., Friel E. D., Phelps R. L., 1997, AJ, 113, 1723
Kayser A., Hilker M., Grebel E. K., Willemsen P. G., 2008, A&A, 486, 437
Kruijssen J. M. D., 2015, MNRAS, 454, 1658
Lardo C. et al., 2012, A&A, 541, A141
Lardo C. et al., 2013, MNRAS, 433, 1941
Lardo C., Bellazzini M., Pancino E., Carretta E., Bragaglia A., Dalessandro E., 2011, A&A, 525, A114
Larsen S. S., Strader J., Brodie J. P., 2012, A&A, 544, L14
Mackey A. D., Broby Nielsen P., 2007, MNRAS, 379, 151
Martocchia S. et al., 2017, MNRAS, 468, 3150
Martocchia S. et al., 2018a, MNRAS, 477, 4696
Martocchia S. et al., 2018b, MNRAS, 473, 2688
Milone A. P., Bedin L. R., Piotto G., Anderson J., 2009, A&A, 497, 755
Milone A. P. et al., 2017, MNRAS, 464, 3636
Mucciarelli A., Origlia L., Ferraro F. R., Pancino E., 2009, ApJ, 695, L134
Mucciarelli A., Dalessandro E., Ferraro F. R., Origlia L., Lanzoni B., 2014, ApJ, 793, L6
Niederhofer F. et al., 2017, MNRAS, 465, 4159
Niederhofer F., Georgy C., Bastian N., Ekström S., 2015, MNRAS, 453, 2070
Norris J., Cottrell P. L., Freeman K. C., Da Costa G. S., 1981, ApJ, 244, 205
Pancino E., 2018, A&A, 614, A80
Pancino E., Rejkuba M., Zoccali M., Carrera R., 2010, A&A, 524, A44
Piatti A. E., Keller S. C., Mackey A. D., Da Costa G. S., 2014, MNRAS, 444, 1425
Pietrinferni A., Cassisi S., Salaris M., Castelli F., 2006, ApJ, 642, 797
Piotto G. et al., 2015, AJ, 149, 91
Platais I., Cudworth K. M., Kozhurina-Platais V., McLaughlin D. E., Meibom S., Veillet C., 2011, ApJ, 733, L1
Renzini A. et al., 2015, MNRAS, 454, 4197
Schiavon R. P., Caldwell N., Conroy C., Graves G. J., Strader J., MacArthur L. A., Courteau S., Harding P., 2013, ApJ, 776, L7
Simioni M., Milone A. P., Bedin L. R., Aparicio A., Piotto G., Vesperini E., Hong J., 2016, MNRAS, 463, 449
Simpson J. D., De Silva G., Martell S. L., Navin C. A., Zucker D. B., 2017, MNRAS, 472, 2856
Stetson P. B., 1987, PASP, 99, 191
van Dokkum P. G., 2001, PASP, 113, 1420
Vollmann K., Eversberg T., 2006, Astron. Nachr., 327, 862
Worthey G., 1994, ApJS, 95, 107

This paper has been typeset from a TEX/LATEX file prepared by the author.